Isopycnal Stirring and Diapycnal Mixing in the Eastern North Atlantic Inferred from Argo Observations

ESPE BROULLÓN,[a] BIEITO FERNÁNDEZ CASTRO,[a] ALBERTO C. NAVEIRA GARABATO,[a] LOUIS CLÉMENT,[b] MARILENA OLTMANNS,[b,c,d] AND RICHARD G. WILLIAMS[e]

[a] *Ocean and Earth Science, National Oceanography Centre, University of Southampton, Southampton, United Kingdom*
[b] *National Oceanography Centre, Southampton, United Kingdom*
[c] *University of Bremen, Bremen, Germany*
[d] *Alfred Wegener Institute, Bremerhaven, Germany*
[e] *Earth, Ocean and Ecological Sciences, School of Environmental Sciences, University of Liverpool, Liverpool, United Kingdom*

(Manuscript received 28 April 2025, in final form 24 November 2025, accepted 5 January 2026)

ABSTRACT: The variability of isopycnal stirring and diapycnal mixing associated with mesoscale and microscale turbulence, respectively, is assessed using Argo float observations in the eastern subtropical North Atlantic. A new method is introduced combining a finescale parameterization with a triple decomposition framework to separate isopycnal stirring and diapycnal mixing. Our approach is validated by comparing with microstructure measurements from an independent North Atlantic tracer release experiment in the 1990s. Both sets of diagnostics reveal that diapycnal mixing dominates in the upper thermocline and that isopycnal stirring prevails in deeper, intermediate layers, influenced by Mediterranean Outflow Water. The analysis of Argo data for years 2014–24 reveals substantial interannual variations in stirring and mixing rates and in the relative contributions of mesoscale and microscale processes to thermohaline variance dissipation, which persisted in time (~3 yr) and across isopycnal layers (26.75–27.5 kg m^{-3}). A shift in the relative contributions to the variance dissipation occurred over the period, with more prevalent isopycnal stirring in the thermocline after 2018. This enhancement of isopycnal stirring, which concurred with lower isopycnal diffusivities, is attributed to increased property gradient along-isopycnals induced by a large-scale cooling and freshening of the eastern subtropical North Atlantic. Our results highlight how property contrasts in the thermocline, induced originally by ocean ventilation, are modified by isopycnal stirring and diapycnal mixing. This application of finescale parameterizations constitutes a powerful tool that has the potential to capture and quantify the temporal evolution of isopycnal stirring and diapycnal mixing rates from Argo observations across the global ocean.

SIGNIFICANCE STATEMENT: Ocean ventilation is vital in the climate system, transferring fluid and properties from the surface to the ocean interior. Yet, the ways in which stirring and mixing modulate ventilation are poorly understood, due to the sparseness of small-scale ocean observations. By applying a novel approach to Argo float data, we diagnose stirring and mixing processes in the subtropical North Atlantic over a recent decade. Our results reveal a shift after 2018, with mesoscale stirring becoming more dominant in response to a major cooling and freshening event. The enhanced stirring dampens temperature and salinity contrasts, thus distributing the effects of externally forced, large-scale changes across the North Atlantic. Our study opens new opportunities to diagnose stirring and mixing across the global ocean.

KEYWORDS: North Atlantic Ocean; Diapycnal mixing; Mixing; Turbulence; Isopycnal mixing; Ventilation

1. Introduction

Ocean mixing, involving stirring and homogenization of tracers by mesoscale and microscale ocean turbulence, plays a fundamental role in shaping property distributions in the ocean interior (De Lavergne et al. 2021; Munk and Wunsch 1998). For example, in the thermocline (Iselin 1939), temperature and salinity are initially determined by ventilation from the winter mixed layer (Stommel 1979; Williams et al. 1995) involving subduction within the subtropical gyres (Luyten et al. 1983; Williams 1991; Marshall et al. 1993; MacGilchrist et al. 2017). These subducted properties may then be altered by mesoscale eddy-induced isopycnal stirring and diapycnal mixing due to microscale turbulence in the ocean interior (Robbins et al. 2000). However, the sparseness of microstructure observations makes it difficult to assess the competition between subduction and stirring/mixing in determining the properties of the subtropical thermocline. Direct measurements of irreversible mixing are restricted to isolated observations over limited oceanic areas and periods (Waterhouse et al. 2014). Alternatively, a range of approaches combining theory and observational in situ and remote sensing data has been used to produce global maps of isopycnal and diapycnal diffusivities. However, with a few exceptions (Busecke and Abernathey 2019), these approaches have not yet been used to represent interannual or decadal changes in dissipation rates of isopycnal—stirring—and diapycnal—mixing—variances (Cole et al. 2015; Groeskamp et al. 2020).

Denotes content that is immediately available upon publication as open access.

Corresponding author: Espe Broullón, e.broullon-mandado@soton.ac.uk

DOI: 10.1175/JPO-D-25-0090.1

An additional challenge is that mesoscale isopycnal stirring and microscale diapycnal mixing processes operate at different spatiotemporal scales and are measured or estimated using different methodological approaches. While dissipation rates of variance—here, mixing rates—by microscale turbulence are routinely measured directly using microstructure observations of temperature and shear (Waterhouse et al. 2014; Lueck et al. 2024), isopycnal stirring by mesoscale turbulence is usually quantified by inferring values of isopycnal diffusivity, often via indirect techniques (Abernathey et al. 2022), such as mixing-length theory (Naveira Garabato et al. 2011; Cole et al. 2015; Groeskamp et al. 2020). Alternatively, direct estimates can be obtained from real or simulated tracer/float release experiments (Abernathey and Marshall 2013; Tulloch et al. 2014; Rudnickas et al. 2019).

The relative importance of variance dissipation via isopycnal and diapycnal processes in determining property distributions in the ocean is largely unconstrained by observations, since this comparison has only been quantified concurrently in a few studies, which combine microstructure observations with the triple decomposition of the variance equation (Ferrari and Polzin 2005; Naveira Garabato et al. 2016; Fernández Castro et al. 2024). Historically, the availability of direct microscale observations has led to a focus on quantifying diapycnal mixing (Polzin et al. 1997; Waterhouse et al. 2014; Kunze 2017). Yet, isopycnal stirring, involving the filamentation of tracers along density surfaces, is particularly effective for the homogenization of property contrasts. Indeed, isopycnal stirring has been shown to drive vigorous thermohaline water mass transformations in regions of ventilation, such as the subpolar North Atlantic (Fernández Castro et al. 2024; Sijp et al. 2006) and the Southern Ocean (Naveira Garabato et al. 2016; Orúe-Echevarría et al. 2023), and to control the distributions of oxygen, nutrients, and greenhouse gases in the ocean interior, modulating air–sea carbon fluxes, nutrient redistribution, and long-term carbon sequestration (Gnanadesikan et al. 2015; Rudnickas et al. 2019; Bahl et al. 2019; Spingys et al. 2021).

To overcome limitations in measurements of diapycnal mixing, shear- and strain-based finescale parameterizations have been widely used in recent decades. These approaches estimate turbulent kinetic energy dissipation rates and diapycnal diffusivities from routine ship- or float-based hydrographic observations of temperature, salinity, and velocity shear (Whalen et al. 2012; Kunze et al. 2006; Polzin et al. 2014; Kunze 2017; Whalen et al. 2018). Despite their known shortcomings, such as only capturing mixing driven by internal wave breaking, these approaches use finescale data that are much more abundant than microstructure observations, especially since the onset of the Argo float program in 1999 (Wong et al. 2020). As a result, finescale parameterizations have advanced our understanding of diapycnal mixing variability in space and time (Sheen et al. 2014; Whalen et al. 2018; Li et al. 2023). However, these parameterizations have not yet been used to diagnose isopycnal stirring or to compare its relative importance with diapycnal mixing.

Here, we propose and ground-truth a new approach to diagnose both isopycnal stirring and diapycnal mixing rates from finescale data obtained by Argo floats. The proposed method combines (i) the strain-based finescale parameterization (Whalen et al. 2012) to estimate diapycnal diffusivity and the rate of irreversible tracer mixing using the Osborn and Cox (1972) formula with (ii) a triple decomposition framework for the tracer variance equation to assess the contribution of mesoscale, isopycnal stirring (Ferrari and Polzin 2005; Naveira Garabato et al. 2016). Our approach is applied to the eastern subtropical North Atlantic and validated by comparing the obtained estimates with independent microstructure measurements from the 1990s (Ferrari and Polzin 2005; Cherian et al. 2024; Whalen et al. 2012). By performing our analysis on Argo float data from years 2014 to 2024, we reveal substantial temporal fluctuations in stirring and mixing rates, associated with large-scale water mass property changes linked to climate variability. There are also notable variations in the relative importance of mesoscale and microscale turbulence in modifying the characteristics of waters subducted into the thermocline of the subtropical North Atlantic.

In summary, we present and ground-truth a method that enables the estimation of the isopycnal and diapycnal contributions to irreversible tracer mixing. Our results here demonstrate the critical role of mixing and stirring in propagating and dissipating large-scale climate signals across the North Atlantic. In addition, the approach can straightforwardly be applied to globally available finescale ocean data. Thus, the approach represents a powerful tool for characterizing the spatiotemporal variability of stirring and mixing and for assessing their impacts on the oceanic distributions of temperature, salinity, and other tracers over the global ocean.

2. Methods

a. *Observations*

1) NATRE DATASET: MICROSTRUCTURE AND FINE STRUCTURE

Microstructure and CTD observations were collected under the North Atlantic Tracer Release Experiment (NATRE), carried out in April 1992 (Ledwell et al. 1998), using a High Resolution Profiler (HRP; Schmit et al. 1988) and an Neil Brown Instrument Systems (NBIS) Mark III CTD sensor (Ferrari and Polzin 2005). The dataset comprises 150 profiles to depths of up to 2000 m of temperature T, salinity S, pressure and dissipation rates of thermal variance χ_Θ, and turbulent kinetic energy ε, with a vertical resolution of 0.5 dbar. These profiles were contained in a domain in the eastern North Atlantic with coordinates 24°–28°N, 26.5°–31°W, southwest of the Canary Islands (Fig. 1).

Conservative Temperature Θ and Absolute Salinity S_A were evaluated using the Gibbs Seawater (GSW) Oceanographic Toolbox of Thermodynamic Equation of Seawater 2010 (TEOS-10). Neutral density γ^n was calculated using the routines of Jackett and McDougall (1997). Hydrographic data were averaged on a vertical grid with a resolution of 2 m. Vertical gradients of temperature and salinity were calculated by averaging their values within 2-m-thick half-overlapping windows above and below each depth bin and computing finite differences between averages to obtain $\partial\Theta/\partial z \approx \Delta\Theta/\Delta z$. The

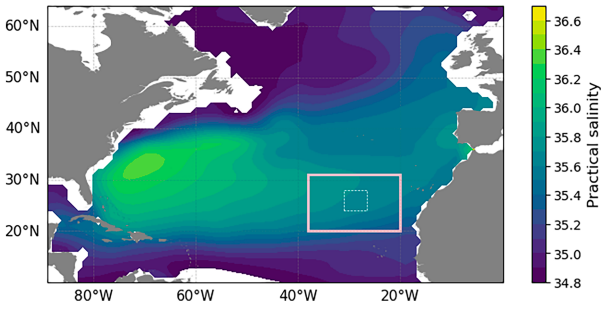

FIG. 1. Map of the subtropical North Atlantic. Background color indicates annual-mean practical salinity at 540-m depth, obtained from EN4 reanalysis data, the fourth generation of the Met Office Hadley Centre's ensemble-based gridded temperature and salinity (Good et al. 2013). Pink box indicates the area where Argo float profiles were selected (20°–31°N, 20°–38°W). White dashed box indicates the area where microstructure observations were collected during NATRE experiment in 1992 (Ledwell et al. 1998).

buoyancy frequency N was derived from the vertical gradient of neutral density γ^n.

The diapycnal diffusivity K_ρ was calculated, using the Osborn (1980) formula, from the turbulent kinetic energy dissipation rate ε and the squared buoyancy frequency N^2:

$$K_\rho = \Gamma \frac{\varepsilon}{N^2}, \tag{1}$$

where Γ is the mixing efficiency, assumed to take a constant value of 0.2 (Oakey 1982).

Measurements of thermal variance dissipation χ_Θ were obtained directly with microstructure temperature observations. To derive haline variance dissipation rates χ_{S_A}, which are not directly measured, we used the Osborn–Cox relation (Osborn and Cox 1972):

$$\chi_{S_A} \approx P_{S_A^2} \approx 2K_\rho \left(\frac{\partial S_A}{\partial z}\right)^2, \tag{2}$$

where $\partial S_A/\partial z$ is the vertical gradient of Absolute Salinity calculated on the averaged vertical grid of 2-m resolution. This approximation to estimate variance dissipation assumes a local balance between the production of tracer variance by small-scale turbulence, denoted $P_{S_A^2}$, and its dissipation by molecular diffusion, χ_{S_A} (Fernández Castro et al. 2024). The approximation is based on the tracer variance conservation equation and assumes steady state and zero convergence of the variance transport terms. It has been found to approximate the measured thermal dissipation within a factor of 2 in the subpolar and subtropical North Atlantic (Fernández Castro et al. 2024).

2) ARGO FLOATS: CTD FINE STRUCTURE

Temperature and salinity profiles from Argo floats were obtained within a wider region (20°–31°N, 20°–38°W) surrounding the NATRE sampling area between years 2014 and 2024 (Fig. 1).

The use of the Osborn and Cox (1972) formula to infer variance dissipation rates requires that vertical gradients are accurately resolved on relatively fine scales (<10 m). Therefore, only Argo profiles with a mean vertical resolution finer than 5 m were used. Data prior to 2014 failed to meet that requirement too often, particularly below 1000 m, and were not considered. For the 2014–24 period, 7079 Argo CTD profiles were available. Data were averaged on a vertical grid with a resolution of 2 m, where their vertical gradients as well as neutral density γ^n and squared buoyancy frequency N^2 were calculated. In measurements with coarse grid spacing, the resulting gridded profiles will exhibit gaps.

b. *Finescale parameterization: Diffusivity and dissipation rates*

Turbulent kinetic energy dissipation rates ε and diapycnal diffusivity K_ρ were estimated for both datasets (NATRE and Argo) using the 2-m gridded CTD data. The strain-based finescale parameterization (Whalen et al. 2012; Kunze et al. 2006) was implemented with the *mixsea* Python package (Voet et al. 2023) which returns ε and K_ρ for predefined vertical segments (appendix A). Calculations for each profile were performed at depth bins separated by 50 m with a window size of 200 m, so that each window for each bin overlaps with the previous and the following ones by 150 m. Spectral calculations were done over a wavenumber range spanning between a wavelength equal to half the window size of 200 m and a minimum wavelength size of 10 m. As Argo floats do not have velocity data to calculate shear, a constant value for the shear to strain ratio R_ω was set to 3, equal to the Garrett–Munk estimate. This choice has been found to perform adequately around the NATRE region (Kunze et al. 2006; Whalen et al. 2012). Depth bins in which the mean resolution was >10 m were not considered.

Variance dissipation rate estimates for Conservative Temperature χ_Θ and salinity χ_{S_A} were obtained through Eq. (2) (Osborn and Cox 1972), using the diapycnal diffusivity values derived from the finescale parameterization. Variance dissipation rates, χ_Θ and χ_{S_A}, were calculated over the 200-m bins as

$$\chi_\Theta \approx 2K_\rho \left(\frac{\partial \Theta}{\partial z}\right)^2, \tag{3}$$

where $(\partial\Theta/\partial z)^2$ is the 2-m-scale vertical gradient of Θ, squared and averaged over 200-m windows.

For the Argo float time series, all mixing-related quantities were averaged onto a time grid with a 3-month time step and a 12-month moving window centered at each time step. For both Argo and NATRE datasets, mixing rates and other variables were averaged onto neutral density layers extending from the upper thermocline to intermediate waters (IWs), i.e., between the 26.75 kg m^{-3} (~320 m) and 28.05 kg m^{-3} (~820 m) isopycnals, and spaced by 0.05 kg m^{-3}.

c. *Thermohaline variance budget: Triple decomposition framework*

With the aim of quantifying the relative contributions of mesoscale and microscale turbulence to thermohaline mixing, we

apply a triple decomposition of the variance conservation equation (Ferrari and Polzin 2005; Naveira Garabato et al. 2016). This method decomposes the variability of a tracer (herewith Θ, but the same applies to S_A) into three components: (i) large-scale mean, (ii) mesoscale eddy fluctuations, and (iii) microscale fluctuations (Joyce 1977; Garrett 2001). Mesoscale fluctuations originate from the stirring of tracer contrast along-isopycnals and, therefore, relate to the strength of the isopycnal stirring process (denoted by $\|$), while microscale fluctuations are produced by isotropic small-scale turbulence and relate to the strength of diapycnal mixing (denoted by $\perp$). The decomposition assumes a spectral gap between these scales of the tracer distribution such that Θ is the sum of three terms: $\Theta = \Theta^m + \Theta^e + \Theta^t$, where superscripts m, e, and t refer to the large-scale mean flow, mesoscale, and small-scale turbulence, respectively.

In this framework, the small-scale tracer variance production P_{Θ^2} in the Osborn–Cox relation [Eq. (2)] is separated into two terms: one accounting for the mesoscale fluctuations, equivalent to isopycnal stirring, $P_{\|,\Theta^2}$, and the other accounting for the microscale turbulence, assumed equivalent to diapycnal variance production, $P_{\perp,\Theta^2}$. Thus, the triple variance decomposition of the tracer is expressed as in Ferrari and Polzin (2005) by a balance between production and dissipation of tracer variance,

$$\underbrace{-2\langle \mathbf{u}^t\Theta^t\rangle\cdot\nabla\Theta^m}_{\text{microscale turbulence}}\underbrace{-2\langle \mathbf{u}^e\Theta^e\rangle\cdot\nabla\Theta^m}_{\text{mesoscale eddy}} = \chi_\Theta, \tag{4}$$

where $\langle\rangle$ brackets represent an average over spatiotemporal scales that are large in comparison with mesoscale fluctuations. This equation expresses the steady-state balance between the sum of tracer variance production from microscale diapycnal mixing, $P_{\perp,\Theta^2}$, and mesoscale isopycnal stirring, $P_{\|,\Theta^2}$, and the tracer variance dissipation rate, χ_Θ, neglecting nonsteadiness and variance transport terms:

$$P^{\perp}_{\Theta^2} + P^{\|}_{\Theta^2} = \chi_\Theta. \tag{5}$$

By applying gradient flux approximations, such as $\langle u^t\Theta^t\rangle = -K_\rho\nabla\Theta^m$, and assuming (i) that diapycnal gradients are much larger than isopycnal gradients and (ii) that mesoscale eddies stir tracers preferentially along-isopycnals, such that $2K_\rho(\nabla\Theta^m)^2 \approx 2K_\rho(\nabla_\perp\Theta^m)^2$ and $2K_\|(\nabla\Theta^m)^2 \approx 2K_\|(\nabla_\|\Theta^m)^2$, respectively, Eq. (4) can be written as

$$\underbrace{2K_\rho(\nabla_\perp\Theta^m)^2}_{P^{\perp}_{\Theta^2}} + \underbrace{2K_\|(\nabla_\|\Theta^m)^2}_{P^{\|}_{\Theta^2}} = \chi_\Theta, \tag{6}$$

where $K_\|$ is an isopycnal diffusivity. This expression enables an assessment of how mesoscale and small-scale turbulence contribute to the molecular mixing of heat and freshwater, thus shaping the large-scale ocean's thermohaline structure.

The diapycnal variance production $P^{\perp}_{\Theta^2}$ is diagnosed as

$$P^{\perp}_{\Theta^2} = 2K_\rho(\nabla_\perp\Theta^m)^2 \approx 2K_\rho\left(\frac{\partial\Theta^m}{\partial z}\right)^2, \tag{7}$$

assuming that isopycnal layers are close to horizontal. Here, we estimate mean flow tracer profiles, such as Θ^m, in 3-month intervals, as 12-month running averages on neutral surfaces. Diapycnal gradients, $\partial\Theta^m/\partial z$, are estimated from the averaged tracer profiles.

Mesoscale variance production (i.e., isopycnal stirring), $P^{\|}_{\Theta^2}$, is diagnosed as a residual:

$$P^{\|}_{\Theta^2} = \chi_\Theta - P^{\perp}_{\Theta^2}. \tag{8}$$

Further, Eq. (6) is used to estimate the isopycnal diffusivity $K_\|$ from $P^{\|}_{\Theta^2} = 2K_\|(\nabla_\|\Theta^m)^2$:

$$K_{\|,\Theta} = \frac{\chi_\Theta - P^{\perp}_{\Theta^2}}{2(\nabla_\|\Theta^m)^2}, \tag{9}$$

where the subscript in $K_{\|,\Theta}$ notes that isopycnal diffusivity is derived from temperature observations. An equivalent estimation is done based on salinity. Isopycnal thermohaline gradients ($\nabla_\|\Theta^m$) were calculated for each time step as the slope of a linear fit of Θ (or S_A) versus longitude for x axis and latitude for y axis, respectively, for all the available Argo observations in the study area.

3. Results

a. Method validation

Microstructure observations collected during NATRE revealed a mean diapycnal diffusivity profile, $K_\rho^{\text{NATRE}_{\text{micro}}}$, that increases with depth, with values ranging from $\sim 7\times10^{-6}$ m^2 s^{-1} in thermocline waters (TWs) up to $\sim 10^{-5}$ m^2 s^{-1} at 1800-m depth (Fig. 2a). Diffusivity values obtained by applying the finescale parameterization to each individual profile, $K_\rho^{\text{NATRE}_{\text{FS}}}$, are in excellent agreement with the more direct microstructure estimates. The magnitude and shape of both profiles are comparable, exhibiting a mean absolute deviation of 1.7×10^{-6} m^2 s^{-1}, which represents a difference of ~20% of the data range in the profile obtained from microstructure measurements.

The variance dissipation rates for both Conservative Temperature, χ_Θ^{FS} (where FS denotes the finescale approach), and Absolute Salinity, $\chi_{S_A}^{\text{FS}}$, were calculated by combining the finescale parameterization with the Osborn and Cox (1972) formula and compared with either the measured rate, $\chi_\Theta^{\text{micro}}$, or that derived from the microstructure data with the same approach, $\chi_{S_A}^{\text{micro}}$ (Fig. 2a). For both methods, time-mean χ profiles mostly overlap throughout the vertical coordinate, following the same order of magnitude at each depth. The mean absolute deviation between the two profiles for χ_Θ is 6.2×10^{-10} K^2 s^{-1} and for χ_{S_A} is 1.4×10^{-11} g^2 kg^{-2} s^{-1}, which indicates a difference of ~9% and ~6%, respectively, of the data range in the profiles obtained from microstructure measurements. Both χ_Θ and χ_{S_A} generally decrease with depth, ranging from values for $\chi_\Theta^{\text{micro}}$ of $\sim 7\times10^{-9}$ K^2 s^{-1} and for $\chi_{S_A}^{\text{micro}}$ of $\sim 2\times10^{-10}$ g^2 kg^{-2} s^{-1} in upper thermocline waters down to values for $\chi_\Theta^{\text{micro}}$ of $\sim 3\times10^{-10}$ K^2 s^{-1} and for $\chi_{S_A}^{\text{micro}}$ of $\sim 5\times10^{-12}$ g^2 kg^{-2} s^{-1} at 1800-m depth. Secondary maxima of the dissipation rates were observed at ~1000 m

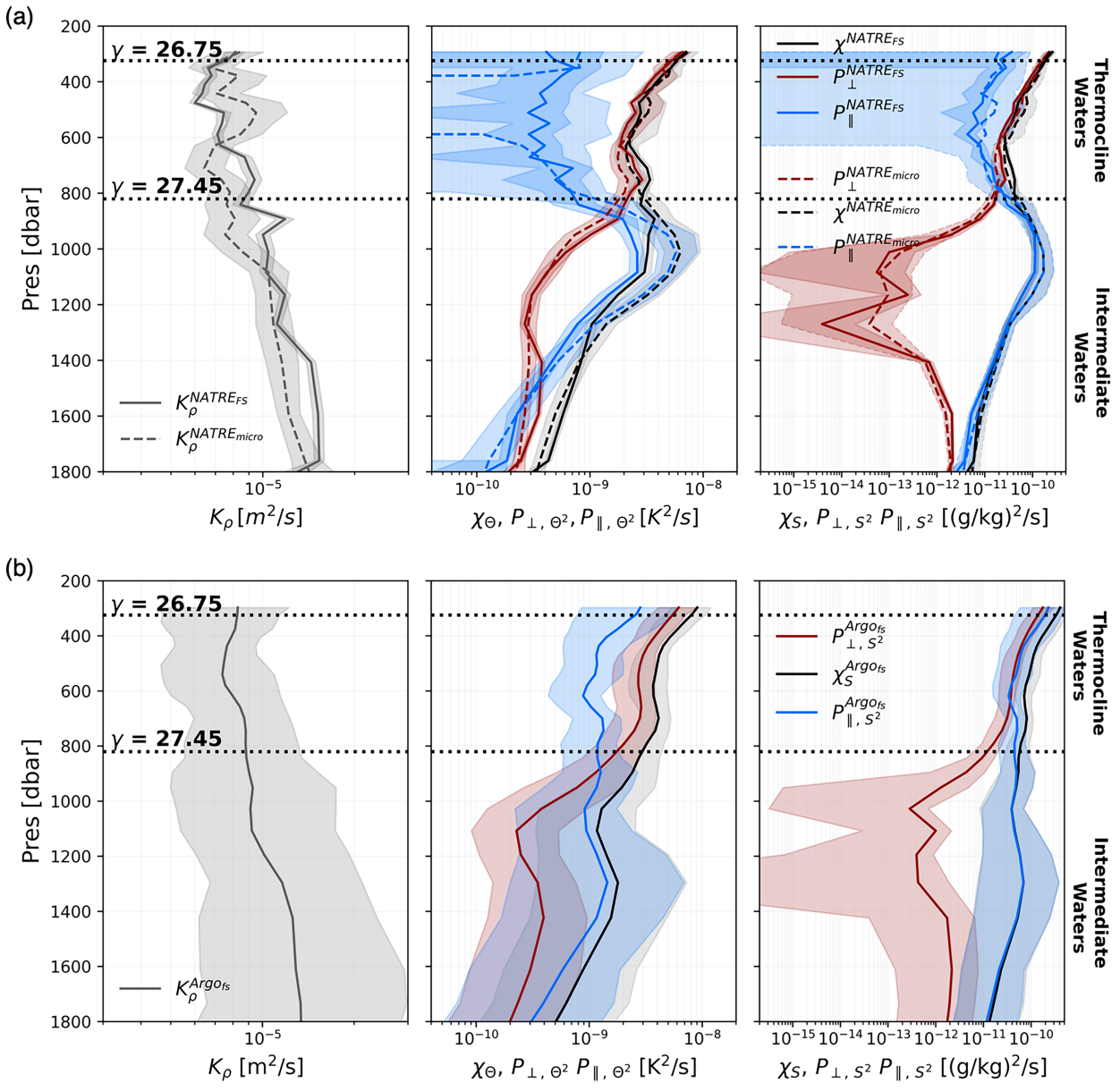

FIG. 2. Mixing diagnostics from (a) NATRE and (b) Argo data. Time-mean profiles of (left) diapycnal diffusivity K_ρ, (center) dissipation rate of thermal variance χ_Θ and its diapycnal $P_{\perp,\Theta^2}$ and isopycnal $P_{\parallel,\Theta^2}$ contributions (black, red, and blue lines, respectively), and (right) dissipation rate of salinity variance χ_{S_A} and its diapycnal $P_{\perp,S_A^2}$ and isopycnal $P_{\parallel,S_A^2}$ contributions. Solid lines refer to microstructure measurements, while dashed lines correspond to values estimated through finescale parameterization applied to CTD data, both datasets from NATRE (Ledwell et al. 1998). Shading areas indicate 95% confidence intervals estimated by bootstrapping on each bin and propagated to residual variables, such as $P_\parallel$ (appendix B).

and associated with the Mediterranean Outflow Water as already shown by Ferrari and Polzin (2005).

The contributions of diapycnal $P_\perp$ and isopycnal $P_\parallel$ productions to the dissipation of tracer variance χ show contrasting vertical distributions across the thermocline ($\gamma^n < 27.45$ kg m^{-3}) and intermediate levels ($\gamma^n > 27.45$ kg m^{-3}); the latter is being influenced by large-scale thermohaline contrasts on isopycnals due to the presence of relatively warm and salty Mediterranean Outflow Water, as previously illustrated by Ferrari and Polzin (2005). Within the thermocline, time-mean diapycnal production $P_\perp$ aligns closely with the total variance dissipation χ for both temperature and salinity. In contrast, in intermediate layers, diapycnal variance production $P_\perp$ decreases to a minimum, with mixing being predominantly supplied by isopycnal variance production $P_\parallel$. The results derived from the finescale parameterization, $\chi^{\mathrm{NATRE_{FS}}}$, $P_\perp^{\mathrm{NATRE_{FS}}}$, and $P_\parallel^{\mathrm{NATRE_{FS}}}$, effectively replicate the features found in microstructure observations.

In spite of the overall good agreement between the two diagnostics—microstructure and finescale parameterization—with their mean profiles lying within the range of the 95% confidence intervals (appendix B), some discrepancies are observed at certain depths in the diffusivity estimates, as well as in the thermal variance budget. At the depth of maximum thermal variance dissipation in the intermediate waters (~1000 m), χ and $P_{\|}$ obtained through the microstructure observations yield values larger than those from the finescale parameterization. In both cases, the diagnostics agree within a factor of ~2. However, according to Oakey (1982), a factor of 2 lies within the expected natural variability of turbulence estimates which usually cover several orders of magnitude and has been commonly accepted in the literature (Goto et al. 2016; Piccolroaz et al. 2021; MacKinnon et al. 2013; Fer et al. 2014).

Analyses of the time-mean profiles from Argo floats (2014–24) resulting from applying the finescale parameterization in the NATRE region (Fig. 2b) are consistent with the original NATRE microstructure results, as well as their finescale observations. There are, however, some differences in the values of the variance production and dissipation rates and in their vertical distribution. Namely, isopycnal stirring appears to make a more important contribution to mixing in the thermocline, both for temperature and salinity. Also, the maxima of mixing rates associated with the intermediate levels are less prominent and located deeper (~1300 m) in the water column in the Argo measurements, compared to the NATRE dataset. Because the same exact methodology is applied to the finescale Argo and NATRE data, a plausible explanation for these differences is due to their temporal coverage: NATRE measurements were collected solely in April 1992, while the Argo dataset spans all seasons for a full, later decade. This potential explanation is explored next. The different sizes of the NATRE box and Argo box [Eq. (1)] might also be contributing to these slight differences in the mean profiles.

b. Variability of mixing rates and regimes during 2014–24

Interannual variability is presented as anomalies with respect to the time mean over the period 2014–24 for the dissipation rates of temperature χ_Θ and salinity variance χ_{S_A} (Figs. 3a,b), as well as for the isopycnal contribution to variance production, $P_{\|,\Theta^2}$ and $P_{\|,S_A^2}$ (Figs. 3c,d). Such rates vary differently across the thermocline and the intermediate levels, and also depending on the tracer.

In thermocline waters, anomalies of variance dissipation rate for temperature χ_Θ and salinity χ_{S_A} show positive values between years 2018 and 2022, more pronounced in the haline component. Although the pattern in this layer is similar for both tracers, anomalies for χ_Θ are also positive at the beginning of the period (2014–17), especially toward deeper isopycnals within the thermocline. In the intermediate layer, χ_Θ and χ_{S_A} display the opposite structure: positive anomalies before 2018 and in 2023. A large relative decay in variance dissipation rate is observed in intermediate layers between 2018 and 2022, coinciding with enhanced mixing in thermocline layers.

A remarkable feature of these time series is that the variability in the isopycnal production of tracer variance, $P_{\|,\Theta^2}$ and $P_{\|,S_A^2}$, exhibits the same tendency as the overall variance dissipation rates, χ_Θ and χ_{S_A}, indicating that variability in mesoscale eddy stirring is the main driver of changes in mixing. There is a clear shift in $P_{\|,\Theta^2}$ and $P_{\|,S_A^2}$ around year 2018 from negative to positive in the thermocline layer and the opposite in intermediate layers. Toward the end of the time series, anomalies in isopycnal stirring within the thermocline become negative and positive in the intermediate waters.

At the beginning of the 10-yr mixing record, the relative contribution of diapycnal mixing to overall variance dissipation in the thermocline is highlighted by the dominance of the diapycnal tracer variance production, $P_\perp$, for both Θ and S_A (~80% for $P_{\perp,\Theta^2}$ and ~64% for $P_{\perp,S_A^2}$). The dominance of the diapycnal contribution decays after 2018, as the isopycnal contribution is more prominent for temperature (where $P_{\perp,\Theta^2}$ contributes with ~65% to χ_Θ) and dominant for salinity ($P_{\perp,S_A^2}$ contributing only ~36% of χ_{S_A}). Variance dissipation within intermediate waters is mostly explained by the isopycnal contribution throughout the study period and for both tracers. Such dominance is especially pronounced toward the end of the time series, with a time mean of ~41% for $P_{\perp,\Theta^2}$ up to 2018, and ~32% after that year, and ~10% for $P_{\perp,S_A^2}$ up to 2018, and ~4% after that year.

c. Drivers of mixing variability

The temporally variable interplay between mesoscale isopycnal and small-scale diapycnal contributions to thermohaline mixing in our study domain raises the question of what processes underpin such changes. Diapycnal and isopycnal mixing rates scale with the product of the diffusivity and tracer gradient squared in the cross- and along-isopycnal directions, respectively. Thus, to decipher the drivers of the variability, we analyze the evolution of diapycnal and isopycnal diffusivities and corresponding tracer gradients over the 2014–24 period.

The highest values of diapycnal diffusivity, K_ρ ($>10^{-5}$ m^2 s^{-1}), are mostly located in intermediate waters, leading to a time-mean profile that increases with depth (Figs. 4a,b). However, periods of low K_ρ values are also observed within that layer, resulting in a more homogeneous K_ρ profile. Notably, K_ρ decreases over time in both thermocline waters and intermediate layers after year 2018, with the latter exhibiting a sharper and slightly delayed decline. Somewhat counterintuitively, the period of reduced diffusivities coincides with enhanced variance dissipation rates in the thermocline (Figs. 3a,b). Toward the end of the time series, after year 2022, K_ρ increases again at some depths including in intermediate waters, resulting in a depth-enhanced diffusivity profile.

The isopycnal diffusivity derived from the temperature variance budget [Eq. (9)], $K_{\|,\Theta}$ (Figs. 4c,d), displays its highest mean values on lighter isopycnals of the thermocline, with median values of ~10^4 m^2 s^{-1}, in broad agreement with the upper range of previous estimates in the region (Ferrari and Polzin 2005; Groeskamp et al. 2020; Cherian et al. 2024; Zika et al. 2010). Below the 27.25 kg m^{-3} isopycnal, $K_{\|,\Theta}$ sharply

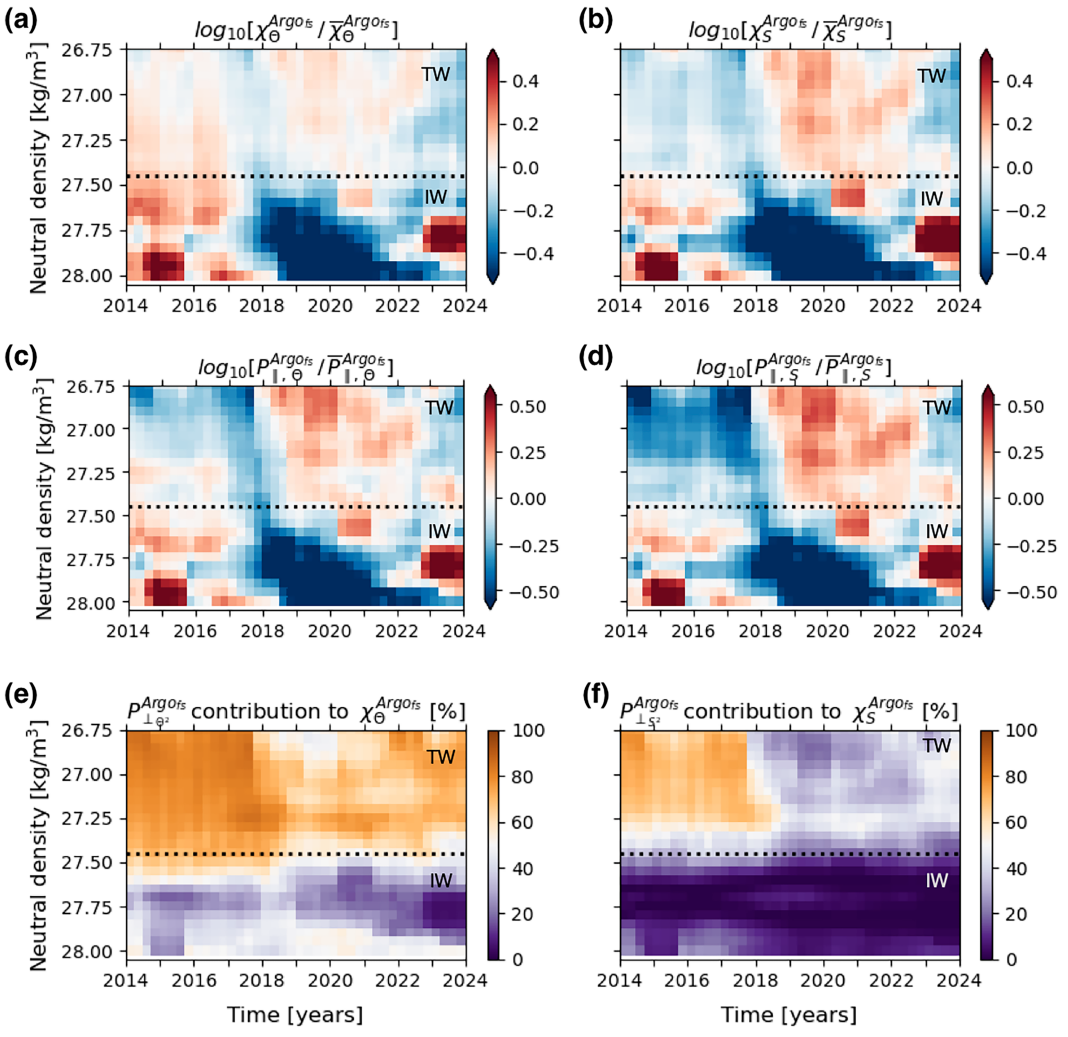

FIG. 3. Mixing variability from Argo observations. Time series (2014–24) of $\log_{10}$ anomalies of the dissipation rate of (a) thermal and (b) haline variance ($\chi/\overline{\chi}$, where overbar denotes a time mean for the study period), time series of (c),(d) $\log_{10}$ anomalies of the thermal and haline isopycnal stirring ($P_{\parallel}/\overline{P_{\parallel}}$), and time series of (e),(f) relative diapycnal contribution (%) to the total dissipation rate of thermal and haline variance, $P_{\perp}/P_{\chi} \times 100$. Anomalies are computed relative to a time mean for each density layer for the study period (2014–24). Horizontal dashed line represents the density boundary between TW ($\gamma < 27.45$ kg m^{-3}) and IW ($\gamma > 27.45$ kg m^{-3}).

decreases by two orders of magnitude, as previously described (Ferrari and Polzin 2005; Cherian et al. 2024). Isopycnal diffusivity derived from the salinity variance budget, $K_{\parallel,S_A}$, is not shown here but closely follows $K_{\parallel,\Theta}$ mean values and variability. Similarly to K_{ρ}, the decrease of isopycnal diffusivity values over years 2018–22 coincides with a period of enhanced thermocline mixing rates. Therefore, the shift in mixing rates can only be explained by enhanced gradients opposing and overcoming reduced diffusivities during that period.

The time-mean squared diapycnal gradient of Θ, $(\nabla_{\perp}\Theta)^2$, decreases with depth, exhibiting largest gradients in the thermocline and at the top of the intermediate layer (Fig. 4e). The temporal trend in $(\nabla_{\perp}\Theta)^2$ reveals significant variability (Fig. 4f). Coinciding with the shift in mixing conditions from years 2018 to 2022, $(\nabla_{\perp}\Theta)^2$ within the thermocline shifts from being associated with negative anomalies relative to the period mean, $(\nabla_{\perp}\Theta)^2 - \overline{(\nabla_{\perp}\Theta)^2}$, to positive anomalies, but the opposite shift occurs in intermediate waters with a change from positive to negative anomalies (Fig. 4j). Toward the end of the time series, $(\nabla_{\perp}\Theta)^2$ returns to being associated with negative anomalies in the lower thermocline.

The time-mean squared isopycnal gradient of Θ, $(\nabla_{\parallel}\Theta)^2$, illustrates more clearly the occurrence of thermohaline isopycnal gradients in intermediate waters, associated with the presence of the Mediterranean Outflow Water, where $(\nabla_{\parallel}\Theta)^2$ reaches a local maximum of $\sim 4 \times 10^{-12}$ K^2 m^{-2} (Fig. 4h). Substantial variability occurs in the time series of $(\nabla_{\parallel}\Theta)^2$ anomalies (Fig. 4g). Again, there is a marked change in $(\nabla_{\parallel}\Theta)^2$ anomalies after 2018, consistent with other variables (Fig. 4) and mixing conditions (Fig. 3). In the thermocline, there is a shift from negative

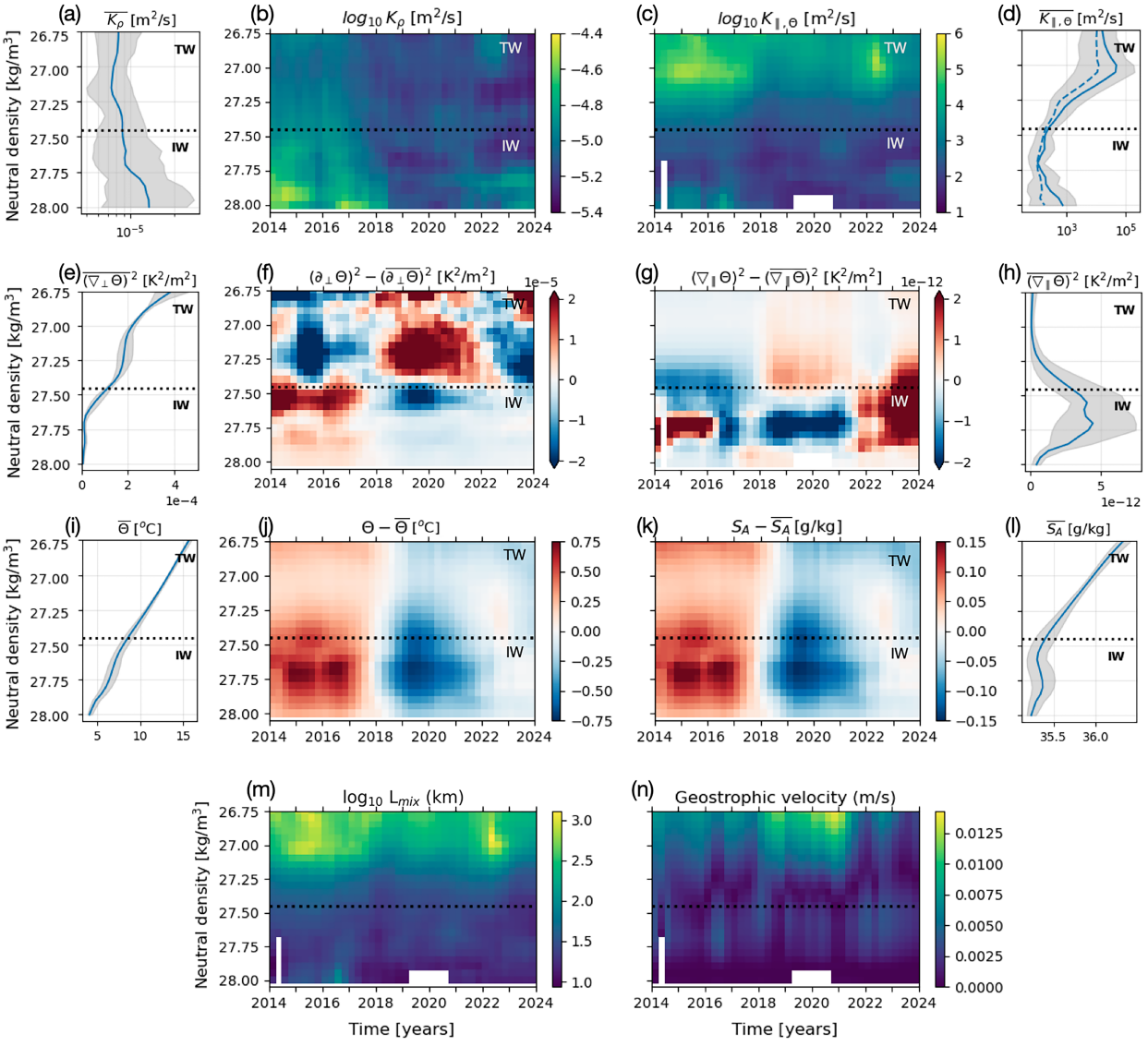

FIG. 4. Drivers of mixing variability. (a) Time-mean () profile and (b) time series (2014–24) of diapycnal diffusivity K_ρ; (c) time series, (d) time-mean (solid line) and time-median (dashed line) profiles of isopycnal thermal diffusivity $K_{\parallel,\Theta}$; (e) time-mean profile of squared vertical Θ gradient, $\nabla_\perp\Theta^2$, and (f) time series of anomalies of squared vertical thermal gradient, $(\partial_\perp\Theta)^2 - \overline{(\partial_\perp\Theta)^2}$; (g) time series of anomalies of horizontal squared Θ gradient, $(\partial_\parallel\Theta)^2 - \overline{(\partial_\parallel\Theta)^2}$, and (h) time-mean profile of squared horizontal Θ gradient $\nabla_\parallel\Theta^2$; (i) time-mean profile of Conservative Temperature, Θ, and (j) time series of Θ anomalies, $\Theta - \overline{\Theta}$; (k) Absolute Salinity anomalies, $S_A - \overline{S_A}$, and (l) time-mean S_A profile; time series of (m) mixing length in $\log_{10}$ (km), calculated as $L_{mix} = \langle S_A^e \rangle^{1/2}/(\nabla_\parallel S_A^m)$, and (n) geostrophic velocity magnitude (m s^{-1}) estimated from isopycnal slopes and referenced to a no-motion level at the deepest observed isopycnal, $\gamma^n \sim 28.05$ kg m^{-3}. Horizontal dashed line represents the density boundary between TW ($\gamma < 26.45$ kg m^{-3}) and IW ($\gamma > 26.45$ kg m^{-3}).

to positive anomalies of the isopycnal thermal gradient over its period mean, $(\nabla_\parallel\Theta)^2 - \overline{(\nabla_\parallel\Theta)^2}$, indicating stronger isopycnal gradients, until negative anomalies return in year 2022. There is a mixture of positive and negative anomalies in intermediate waters, but negative anomalies (indicating weaker gradients) are prevalent from the 2018 shift to 2022, coinciding with when $(\nabla_\parallel\Theta)^2$ anomalies become positive in the thermocline. After that, $(\nabla_\parallel\Theta)^2$ in intermediate waters becomes strongly positive.

The temporal patterns in diapycnal and isopycnal gradients are associated with marked changes in the temperature and salinity distributions on isopycnals occurring during our study period. The time-mean profile of Θ gradually decreases from ~15.7°C at 26.75 kg m^{-3} to ~4.1°C at the 28.00 kg m^{-3} isopycnal (Fig. 4i). Time-mean S_A displays a similar pattern (Fig. 4l), decreasing from its highest values at the top of the thermocline ~36.3 g kg^{-1} to its lowest at the bottom of the profile ~34.2 g kg^{-1}. However, at the core of the intermediate waters, both S_A and Θ exhibit a slight increase associated with Mediterranean Outflow Water influence. Time series of Θ and S_A anomalies (Figs. 4j,k, respectively), calculated as the

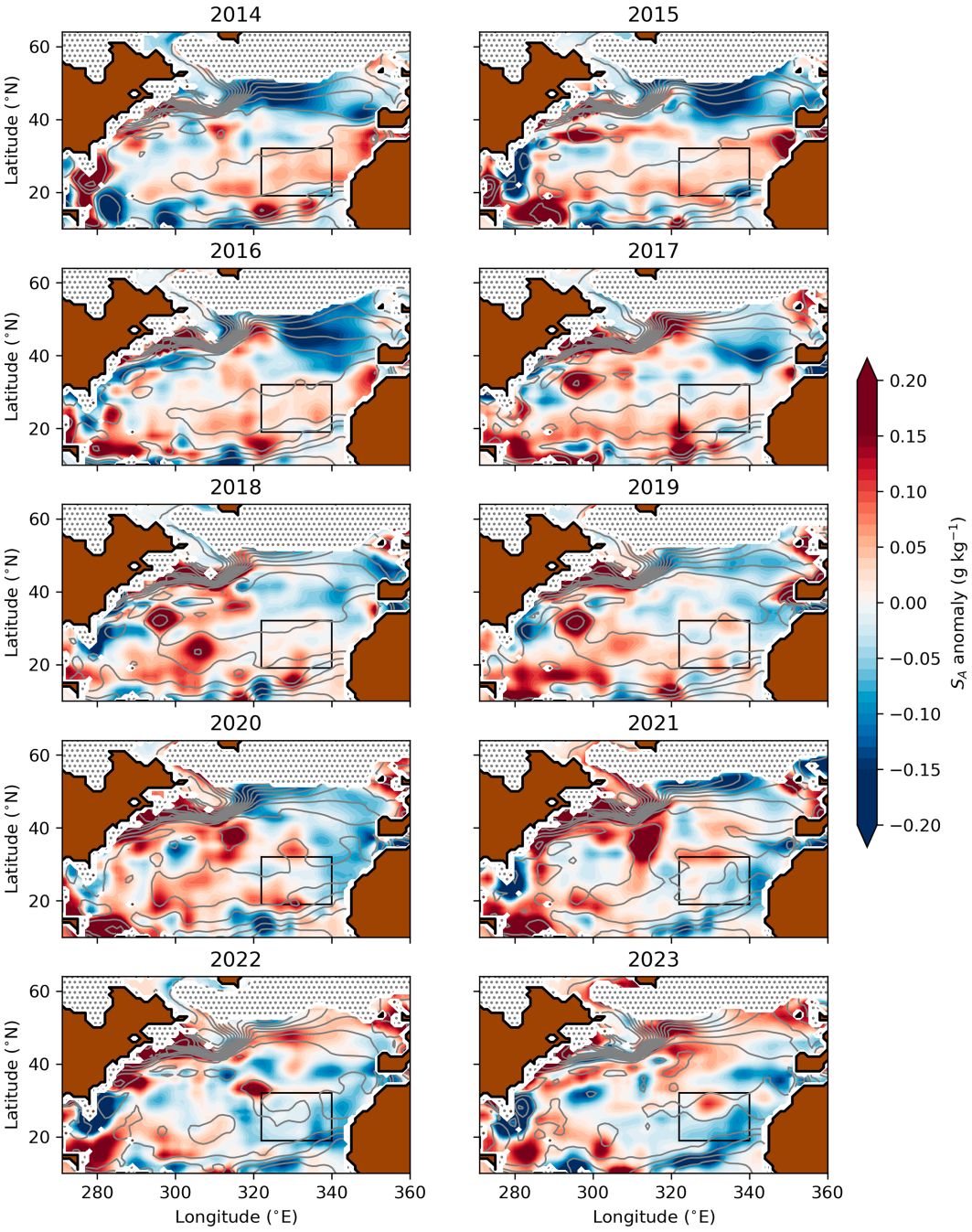

FIG. 5. Large-scale hydrographic changes. Yearly Absolute Salinity anomalies—deviation from the period mean (2000–24)—and annual-mean Absolute Salinity (gray contour lines) in the North Atlantic, at the $\sigma_\Theta = 26.8$ kg m^{-3} surface ($\sigma_\Theta \simeq \gamma^n$) from the observational EN4 product (Good et al. 2013).

difference from time-mean values over the entire period (e.g., $\Theta - \overline{\Theta}$), reveal a shift from positive to negative anomalies, indicating cooler and fresher conditions, after 2018. This change occurs in the entire observed water column, but is more prominent in intermediate layers. By year 2022, negative thermohaline anomalies turn back to almost neutral.

Such shift in thermohaline properties and associated isopycnal gradients can be linked to large-scale changes over the entire North Atlantic. Absolute Salinity anomalies at the 26.8 kg m^{-3} isopycnal—representative of thermocline waters—derived from the EN4 ocean reanalysis reveal a shift from relatively salty to fresher conditions in the eastern subtropical North Atlantic over the period 2014–23 (Fig. 5). At the same time, anomalies of

opposite sign develop in the western subtropical gyre, strengthening salinity and temperature gradient along-isopycnals around our study region. These fresh and cold anomalies originate at the isopycnal's outcrop in the subtropical North Atlantic around 2014–15, as described elsewhere (Josey et al. 2018; Holliday et al. 2020; Oltmanns et al. 2024). The anomalies propagate anticyclonically following the subtropical gyre circulation, reaching the NATRE region around 2018.

4. Discussion and conclusions

Thermohaline properties of the ocean interior are determined through a combination of subduction of waters sourced from the surface mixed layer and the effects of stirring and mixing along and across density surfaces in the ocean interior (MacGilchrist et al. 2017; Robbins et al. 2000; Weller et al. 2004; Lachkar et al. 2007; Gebbie 2007). However, due to the sparsity of mixing observations, the relative roles of stirring and mixing in modulating ocean ventilation are poorly understood. Using Argo floats, we propose a new method to concurrently estimate the rates of isopycnal stirring and diapycnal mixing that result from mesoscale and microscale turbulence, respectively. The method combines a finescale parameterization (Whalen et al. 2012) to calculate diapycnal diffusivities, the Osborn and Cox (1972) formula to estimate tracer variance dissipation rates, and a triple decomposition framework (Ferrari and Polzin 2005) to separate isopycnal and diapycnal contributions to mixing. This approach enabled us to investigate the variability of temperature and salinity mixing in the thermocline and intermediate waters of the eastern subtropical North Atlantic.

First, the method was validated by comparing our finescale diagnostics with microscale measurements from the NATRE experiment in the 1990s (Ledwell et al. 1998). Estimated profiles of the diapycnal mixing and isopycnal stirring rates were in very good agreement with microstructure observations, revealing the dominance of diapycnal mixing in the thermocline and isopycnal stirring in deeper, intermediate levels influenced by Mediterranean Outflow Water as described in Ferrari and Polzin (2005), using independent microstructure measurements.

Although the method successfully reproduces the results from microstructure observations, its applicability might be limited in other areas of the ocean where the underlying assumptions, such as the local balance between variance production and dissipation, might be less accurate. The isopycnal parameters ($P_{\|}$, $K_{\|}$) were derived as residuals from the estimated parameters (χ, $P_{\perp}$); therefore, they may include contributions from neglected processes such as variance advection. As such, the conclusions regarding the isopycnal parameters should be interpreted with some degree of caution.

Our new approach has the potential to reveal temporal variations in the diapycnal and isopycnal contributions to tracer mixing with unprecedented resolution and coverage and unveil their complex drivers. We demonstrated this potential with an analysis of Argo data in the eastern subtropical North Atlantic for the period 2014–24. Our analysis revealed substantial interannual variations in mixing rates and in the relative contributions of mesoscale and microscale processes to variance dissipation. Notably, there was a shift in the mixing regime in the thermocline, with more dominant isopycnal stirring after 2018, particularly for salinity. Counterintuitively, the enhancement in isopycnal stirring rates coincided with a reduction of the isopycnal diffusivity.

The reduction of isopycnal diffusivity between 2018 and 2022 could be explained in terms of mixing length theory (Prandtl 1925; Busecke and Abernathey 2019) according to which isopycnal diffusivity scales as $K_{\|} \sim L_{\mathrm{mix}}\mathrm{EKE}^{1/2}$, where L_{mix} is a mixing length and EKE is the eddy kinetic energy. From Argo observations, we estimated the mixing length as the ratio of the standard deviation of salinity anomalies and the isopycnal gradient, $L_{\mathrm{mix}} \approx \langle S_{\mathrm{A}}^{e\,2}\rangle^{0.5}/|\nabla_{\|} S_{\mathrm{A}}|$ (Cole et al. 2015). The L_{mix} exhibited relatively large values on the order of $\sim 10^3$ km in years 2014–17, 2022, and 2023 but reduced on the order of $\sim 10^2$ km during the period of weak diffusivities from 2018 to 2022 (Fig. 4m). Mixing length suppression was associated with an enhancement of geostrophic velocities (Fig. 4n), which would be qualitatively consistent with mixing suppression by intensified background flow (Ferrari and Nikurashin 2010; Naveira Garabato et al. 2011). However, the increase in the geostrophic velocities (from 0.005 m s^{-1} in years 2014–18 to 0.01 m s^{-1} in years 2018–22) is relatively minor and quantitatively insufficient to explain the observed reduction in mixing length by one order of magnitude. Therefore, further analysis would be required to explain the observed mixing suppression.

The observed strengthening of the geostrophic currents reflects an intensification of the subtropical gyre circulation as suggested by satellite altimetry (Fig. C1 in appendix C), which highlights a positive trend of sea level anomaly (SLA) in the center of the subtropical gyre. This positive pattern indicates a steeper sea surface height gradient and, in turn, stronger geostrophic velocities and strengthened gyre circulation. The North Atlantic Ocean index variability is closely coupled to the large-scale atmospheric circulation over the North Atlantic. Specifically, a higher North Atlantic Oscillation index is associated with a stronger positive wind stress curl in the subpolar region and a more negative wind stress curl anomaly in the subtropical region. This pattern implies that the subpolar and subtropical gyres strengthen simultaneously and are characterized by a stronger zonal North Atlantic Current along with stronger westerlies. Considering, in turn, the high sensitivity of the subpolar gyre circulation to the NAO (Hakkinen and Rhines 2009; Häkkinen et al. 2011, 2013), the strengthening of the ocean currents is consistent with the positive North Atlantic Oscillation phase after 2015 and lasting up to 2023 (Roch et al. 2024; Bhagtani et al. 2025). We also examined the surface EKE variability in the area, but the analysis did not reveal any clear tendency (not shown). Therefore, our findings align with previous work showing that substantial interannual variability in isopycnal diffusivity values is driven by changes in mixing length suppression by variable background flows in response to large-scale climatic forcing (Busecke and Abernathey 2019).

Moreover, the concurrent enhancement of isopycnal stirring and variance dissipation rates was driven by the competing strengthening of temperature and salinity gradients along density surfaces, rather than the magnitude of isopycnal diffusivity.

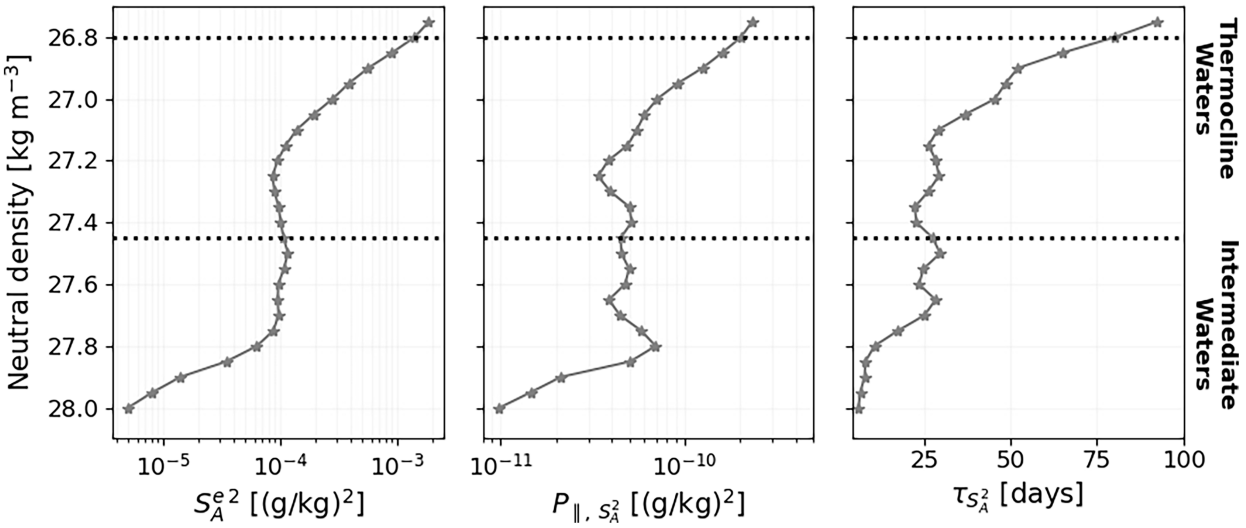

FIG. 6. Inferring time scales of mixing. Time-mean profiles in density space of (left) squared Absolute Salinity mesoscale fluctuations (variance), $\langle S_A^{e\,2}\rangle$, (center) isopycnal salinity variance production, $P_{\parallel,S_A^2}$, and (right) the time scale of the production of mesoscale fluctuations by isopycnal stirring, $\tau_{S_A^{e\,2}}$, calculated as $\tau \sim S_A^{e\,2}/P_{\parallel,S_A^2}$; this estimate is a lower bound as a tracer anomaly may be larger on the mesoscale than the fine scale assumed here.

Gradient intensification was induced by a large-scale cooling and freshening of the eastern rim of the subtropical gyre after 2018. Such freshening followed strong atmospheric forcing and associated shifts in ocean currents at northern latitudes in 2014–16, which caused freshening and cooling in the eastern subtropical North Atlantic (Holliday et al. 2020; Josey et al. 2018). Fresh and cool anomalies subducted along-isopycnals, propagated anticyclonically toward subtropical latitudes, and reached the study area around 2018 (Fig. 5), enhancing the east–west isopycnal temperature and salinity gradients and, thereby, the isopycnal stirring and variance dissipation rates in spite of weaker diffusivities. Thus, the results indicate the importance of isopycnal stirring in equalizing large-scale gradients, effectively facilitating the export and dissipation of salinity and temperature anomalies outside the subpolar North Atlantic.

Although the large-scale freshening and cooling also altered the intermediate levels, gradients and thus mixing trends in these isopycnals were the opposite to those observed in the thermocline. A decline in mixing rates occurred in years 2018–22. In these deeper isopycnals, large-scale preexistent pattern is shaped by southward flow of the Mediterranean waters, which enhances gradients in that direction. The advection of a fresher water mass in the same southward direction reduced property contrasts and thus dissipation rates.

Our novel methodology expands and complements previous research focused on the variability of diapycnal and isopycnal diffusivities, driven by changes in available mechanical energy for turbulence (Whalen et al. 2018; Sheen et al. 2014; Busecke and Abernathey 2019; Li et al. 2023). In turn, our findings highlight the complexity of the interplay between variable diffusivity rates and property gradients in controlling the variability of tracer mixing and irreversible watermass transformations. Our results also have implications for our understanding of how the balance between surface forcing, subduction, and interior mixing ventilates the properties of the thermocline.

Ocean ventilation is widely viewed as determining water mass properties, such as temperature, salinity, and potential vorticity, in the subtropical thermocline via the subduction of surface-modified waters (Luyten et al. 1983; Williams 1991; Marshall et al. 1993). End-of-winter mixed layer properties are thought to be adiabatically transferred into the stratified thermocline (Stommel 1979; Williams et al. 1995; MacGilchrist et al. 2021), with potential modulation by stirring and mixing processes (Robbins et al. 2000; MacGilchrist et al. 2017). To gauge the importance of diapycnal mixing and isopycnal stirring in modifying ventilated properties in the thermocline, we estimate the mixing time scale, $\tau_{S_A^{e\,2}}$—the characteristic time required for stirring and mixing to create and dampen tracer anomalies (Naveira Garabato et al. 2016). The $\tau_{S_A^{e\,2}}$ is computed as the ratio of the mesoscale salinity variance (here, density-compensated vertical fine structure), $\langle S_A^{e\,2}\rangle$, and the rate of production by mesoscale stirring, $P_{\parallel,S_A^2}$:

$$\tau_{S_A^{e\,2}} \sim \frac{\langle S_A^{e\,2}\rangle}{P_{\parallel,S_A^2}}. \tag{10}$$

This time scale for the production and dampening of interleaving finescale anomalies (Fig. 6) ranges from typically 25 to 75 days in the thermocline. This damping time scale should be viewed as a lower bound for how long mesoscale tracer anomalies take to be eroded, as the tracer anomalies on the mesoscale may be larger than those observed as finescale interleaving structures.

Thus, the lifetime of interleaving finescale structures resulting from the stirring processes is typically months, which is comparable to the characteristic seasonal and longer time

scales of the subduction process (Williams et al. 1995; Marshall et al. 1993) and shorter than the time scale of advection from remote source regions, as shown in Fig. 5. This scaling suggests that stirring rates react to changes in thermohaline gradient along isopycnals, as might occur from interannual variations in the properties of waters subducted into the thermocline, on subseasonal time scales. Such relatively rapid response of stirring and mixing rates to surface-forced hydrographic changes indicates that isopycnal stirring and diapycnal mixing effectively dampen temperature–salinity anomalies produced by upstream subduction. Therefore, our findings are consistent with the notion that thermohaline properties in the thermocline are determined by an interplay between subduction processes, which enhance property contrasts, and stirring and mixing processes, which mitigate property contrasts.

In summary, a new methodology is introduced to estimate diapycnal and isopycnal mixing rates from finely resolved CTD data. The method accurately reproduces microstructure-based mixing observations in the subtropical eastern North Atlantic. Using the new method, our analysis of Argo data in the same region reveals a shift in thermohaline properties forced by large-scale climate variability. This climate-induced shift interacted with the different large-scale circulation patterns characterizing the thermocline and the intermediate waters leading to opposite mixing responses. The shift in water-mass properties induces changes in mixing conditions and in the relative contributions of mesoscale and microscale processes to variance dissipation as mixing rates adjust to smooth out property anomalies advected to the thermocline induced by climate forcing. These results demonstrate the feasibility and benefits of applying our approach to the global Argo array, to quantify isopycnal stirring and diapycnal mixing rates at unprecedented spatiotemporal scales.

Acknowledgments. This work was supported by a U.K. Natural Environment Research Council Grant NE/W009501/1 (C-Streams). B. F. C. is supported by a European Research Council-Consolidator Grant 101169952 (REMIX-TUNE), and by an Advanced Research and Invention Agency-Forecasting Tipping Points Grant SCOP-PR01-P021 (POLEMIX).

Data availability statement. Argo float data were downloaded using *argopy* (https://argopy.readthedocs.io/) on a "research" mode. Microstructure data were downloaded from https://microstructure.ucsd.edu/. EN4.2.2 product hydrographic observational data for the North Atlantic were downloaded from https://www.metoffice.gov.uk/hadobs/en4/. Sea level anomalies were computed using Copernicus Marine Service dataset cmems_obs-sl_glo_phy-ssh_my_allsat-l4-duacs-0.25deg_P1M-m available at https://data.marine.copernicus.eu/product/SEALEVEL_GLO_PHY_L4_MY_008_047/services.

APPENDIX A

Finescale Parameterization for Turbulent Kinetic Energy Dissipation

Following Whalen et al. (2012), a finescale parameterization for turbulent kinetic dissipation is applied to Argo data. Strain ξ_z was diagnosed from the buoyancy frequency N from the Argo data:

$$\xi_z = \frac{N^2 - N^2_{\text{fit}}}{\overline{N^2}}, \tag{A1}$$

where the overbar represents a vertical averaging and N_{fit} is a quadratic fit to the buoyancy frequency. The strain variance $\langle \xi_z \rangle$ was evaluated after a spatial Fourier transform of the data. Following Kunze et al. (2006), the turbulent kinetic energy dissipation rate ϵ was diagnosed using the strain variance in a finescale parameterization:

$$\epsilon = \epsilon_o \frac{\overline{N^2}}{N_o^2} \frac{\langle \xi_z^2 \rangle^2}{\langle \xi_{z\text{GM}}^2 \rangle^2} h(R_\omega) L(f, N), \tag{A2}$$

where the constants $\epsilon_o = 6.73 \times 10^{-10}$ m^2 s^{-2} and $N_o = 5.24 \times 10^{-3}$rad s^{-1}; the function $L(f, N)$ provides a latitudinal correction depending upon the Coriolis parameter f and the buoyancy frequency N; and $h(R_\omega)$ depends on the frequency content of the internal wave field, varying with the shear to strain ratio R_ω.

The diapycnal diffusivity K_ρ is then diagnosed using the ratio of the turbulent kinetic energy dissipation rate and the squared buoyancy frequency from the Argo data using the Osborn (1980) relationship [Eq. (1)].

APPENDIX B

Estimates of Uncertainties in the Tracer Variance Budget

Uncertainties in mixing diagnostics from both microstructure and finescale parameterizations were estimated, following Ferrari and Polzin (2005), by applying a bootstrapping approach (Efron 1982). For each bin, corresponding to an isopycnal layer ($\gamma^n = 0.05$) and a time, we aggregated all data points within the density class, latitude and longitude box, and, in the case of the Argo dataset, the 12-month time window. Uncertainties were estimated by bootstrapping on each bin for ϵ and the derived variables (K_ρ, χ, $P_\perp$, and $P_\parallel$). The number of bootstrap iterations was $n = 1000$, and the number of effective samples on each bin, n_{eff}, was estimated as

$$n_{\text{eff}} = \frac{n_d}{2L_{\text{autocorr}}/\Delta z}, \tag{B1}$$

where n_d is the number of data points within each bin, Δz is the vertical grid spacing, and L_{autocorr} is the autocorrelation length scale of mixing data (i.e., ϵ) which is the length scale of independent vertical segments. From the resulting distributions, we extracted the 95% confidence intervals and calculated the mean profiles. For the case of isopycnal production, $P_\parallel$, which is calculated as a residual of $\chi - P_\perp$, uncertainties were propagated by computing the residual of the distributions and extracting the 2.5th and 97.5th percentiles.

APPENDIX C

Annual-Mean Sea Level Anomalies

Figure C1 shows the annual-mean sea level anomalies with respect to the average of the period 2000–23.

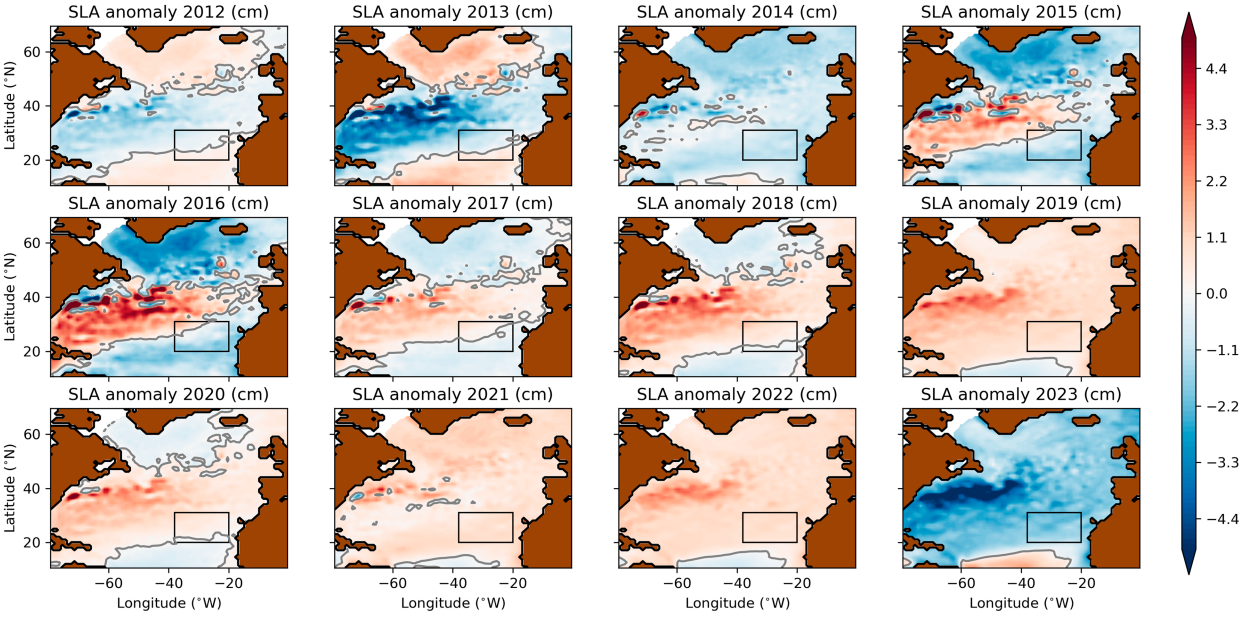

FIG. C1. Annual-mean sea level anomalies with respect to the average of the period 2000–23, from the monthly merged Copernicus Marine Service dataset cmems_obs-sl_glo_phy-ssh_my_allsat-l4-duacs-0.25deg_P1M-m. To isolate large-scale sea level variations, anomalies are computed from a smoothed SLA field reconstructed using the first two empirical orthogonal functions of the SLA fields.

REFERENCES

Abernathey, R., A. Gnanadesikan, M.-A. Pradal, and M. A. Sundermeyer, 2022: Isopycnal mixing. *Ocean Mixing*, Elsevier, 215–256, https://doi.org/10.1016/B978-0-12-821512-8.00016-5.

Abernathey, R. P., and J. Marshall, 2013: Global surface eddy diffusivities derived from satellite altimetry. *J. Geophys. Res. Oceans*, **118**, 901–916, https://doi.org/10.1002/jgrc.20066.

Bahl, A., A. Gnanadesikan, and M. Pradal, 2019: Variations in ocean deoxygenation across Earth system models: Isolating the role of parameterized lateral mixing. *Global Biogeochem. Cycles*, **33**, 703–724, https://doi.org/10.1029/2018GB006121.

Bhagtani, D., A. McC. Hogg, R. M. Holmes, N. C. Constantinou, and H. Khatri, 2025: Asymmetric response of the North Atlantic gyres to the North Atlantic Oscillation. *J. Geophys. Res. Oceans*, **130**, e2024JC021997, https://doi.org/10.1029/2024JC021997.

Busecke, J. J. M., and R. P. Abernathey, 2019: Ocean mesoscale mixing linked to climate variability. *Sci. Adv.*, **5**, eaav5014, https://doi.org/10.1126/sciadv.aav5014.

Cherian, D. A., Y. Guo, and F. O. Bryan, 2024: Assessing modeled mesoscale stirring using microscale observations. *J. Phys. Oceanogr.*, **54**, 1183–1194, https://doi.org/10.1175/JPO-D-23-0135.1.

Cole, S. T., C. Wortham, E. Kunze, and W. B. Owens, 2015: Eddy stirring and horizontal diffusivity from Argo float observations: Geographic and depth variability. *Geophys. Res. Lett.*, **42**, 3989–3997, https://doi.org/10.1002/2015GL063827.

De Lavergne, C., S. Groeskamp, J. Zika, and H. L. Johnson, 2021: The role of mixing in the large-scale ocean circulation. *Ocean Mixing: Drivers, Mechanisms and Impacts*, Elsevier, 35–63, https://doi.org/10.1016/B978-0-12-821512-8.00010-4.

Efron, B., 1982: *The Jackknife, the Bootstrap, and Other Resampling Plans*. Society for Industrial and Applied Mathematics, 92 pp., https://doi.org/10.1137/1.9781611970319.

Fer, I., A. K. Peterson, and J. E. Ullgren, 2014: Microstructure measurements from an underwater glider in the turbulent Faroe Bank Channel overflow. *J. Atmos. Oceanic Technol.*, **31**, 1128–1150, https://doi.org/10.1175/JTECH-D-13-00221.1.

Fernández Castro, B., and Coauthors, 2024: Isopycnal eddy stirring dominates thermohaline mixing in the upper subpolar North Atlantic. *J. Geophys. Res. Oceans*, **129**, e2023JC020817, https://doi.org/10.1029/2023JC020817.

Ferrari, R., and K. L. Polzin, 2005: Finescale structure of the *T*–*S* relation in the eastern North Atlantic. *J. Phys. Oceanogr.*, **35**, 1437–1454, https://doi.org/10.1175/JPO2763.1.

——, and M. Nikurashin, 2010: Suppression of eddy diffusivity across jets in the Southern Ocean. *J. Phys. Oceanogr.*, **40**, 1501–1519, https://doi.org/10.1175/2010JPO4278.1.

Garrett, C., 2001: Stirring and mixing: What are the rate-controlling processes. *Proc. 12th 'Aha Huliko'a Winter Workshop*, Honolulu, HI, University of Hawai'i at Mānoa, 1–8, https://apps.dtic.mil/sti/tr/pdf/ADP013572.pdf.

Gebbie, G., 2007: Does eddy subduction matter in the Northeast Atlantic Ocean? *J. Geophys. Res.*, **112**, C06007, https://doi.org/10.1029/2006JC003568.

Gnanadesikan, A., M.-A. Pradal, and R. Abernathey, 2015: Isopycnal mixing by mesoscale eddies significantly impacts oceanic anthropogenic carbon uptake. *Geophys. Res. Lett.*, **42**, 4249–4255, https://doi.org/10.1002/2015GL064100.

Good, S. A., M. J. Martin, and N. A. Rayner, 2013: EN4: Quality controlled ocean temperature and salinity profiles and monthly objective analyses with uncertainty estimates. *J. Geophys. Res. Oceans*, **118**, 6704–6716, https://doi.org/10.1002/2013JC009067.

Goto, Y., I. Yasuda, and M. Nagasawa, 2016: Turbulence estimation using fast-response thermistors attached to a free-fall vertical microstructure profiler. *J. Atmos. Oceanic Technol.*, **33**, 2065–2078, https://doi.org/10.1175/JTECH-D-15-0220.1.

Groeskamp, S., J. H. LaCasce, T. J. McDougall, and M. Rogé, 2020: Full-depth global estimates of ocean mesoscale eddy mixing from observations and theory. *Geophys. Res. Lett.*, **47**, e2020GL089425, https://doi.org/10.1029/2020GL089425.

Hakkinen, S., and P. B. Rhines, 2009: Shifting surface currents in the northern North Atlantic Ocean. *J. Geophys. Res.*, **114**, C04005, https://doi.org/10.1029/2008JC004883.

Häkkinen, S., P. B. Rhines, and D. L. Worthen, 2011: Warm and saline events embedded in the meridional circulation of the northern North Atlantic. *J. Geophys. Res.*, **116**, C03006, https://doi.org/10.1029/2010JC006275.

——, ——, and ——, 2013: Northern North Atlantic sea surface height and ocean heat content variability. *J. Geophys. Res. Oceans*, **118**, 3670–3678, https://doi.org/10.1002/jgrc.20268.

Holliday, N. P., and Coauthors, 2020: Ocean circulation causes the largest freshening event for 120 years in eastern subpolar North Atlantic. *Nat. Commun.*, **11**, 585, https://doi.org/10.1038/s41467-020-14474-y.

Iselin, C. O., 1939: The influence of vertical and lateral turbulence on the characteristics of the waters at mid-depths. *Eos, Trans. Amer. Geophys. Union*, **20**, 414–417, https://doi.org/10.1029/TR020i003p00414.

Jackett, D. R., and T. J. McDougall, 1997: A neutral density variable for the world's oceans. *J. Phys. Oceanogr.*, **27**, 237–263, https://doi.org/10.1175/1520-0485(1997)027<0237:ANDVFT>2.0.CO;2.

Josey, S. A., J. J.-M. Hirschi, B. Sinha, A. Duchez, J. P. Grist, and R. Marsh, 2018: The recent Atlantic cold anomaly: Causes, consequences, and related phenomena. *Ann. Rev. Mar. Sci.*, **10**, 475–501, https://doi.org/10.1146/annurev-marine-121916-063102.

Joyce, T. M., 1977: A note on the lateral mixing of water masses. *J. Phys. Oceanogr.*, **7**, 626–629, https://doi.org/10.1175/1520-0485(1977)007<0626:ANOTLM>2.0.CO;2.

Kunze, E., 2017: Internal-wave-driven mixing: Global geography and budgets. *J. Phys. Oceanogr.*, **47**, 1325–1345, https://doi.org/10.1175/JPO-D-16-0141.1.

——, E. Firing, J. M. Hummon, T. K. Chereskin, and A. M. Thurnherr, 2006: Global abyssal mixing inferred from lowered ADCP shear and CTD strain profiles. *J. Phys. Oceanogr.*, **36**, 1553–1576, https://doi.org/10.1175/JPO2926.1.

Lachkar, Z., J. C. Orr, J.-C. Dutay, and P. Delecluse, 2007: Effects of mesoscale eddies on global ocean distributions of CFC-11, CO_2, and $\Delta^{14}C$. *Ocean Sci.*, **3**, 461–482, https://doi.org/10.5194/os-3-461-2007.

Ledwell, J. R., A. J. Watson, and C. S. Law, 1998: Mixing of a tracer in the pycnocline. *J. Geophys. Res.*, **103**, 21 499–21 529, https://doi.org/10.1029/98JC01738.

Li, Z., and Coauthors, 2023: Enhanced turbulent diapycnal mixing in the northern Sargasso Sea inferred from a finescale parameterization. *J. Geophys. Res. Oceans*, **128**, e2023JC020220, https://doi.org/10.1029/2023JC020220.

Lueck, R., and Coauthors, 2024: Best practices recommendations for estimating dissipation rates from shear probes. *Front. Mar. Sci.*, **11**, 1334327, https://doi.org/10.3389/fmars.2024.1334327.

Luyten, J. R., J. Pedlosky, and H. Stommel, 1983: The ventilated thermocline. *J. Phys. Oceanogr.*, **13**, 292–309, https://doi.org/10.1175/1520-0485(1983)013<0292:TVT>2.0.CO;2.

MacGilchrist, G. A., D. P. Marshall, H. L. Johnson, C. Lique, and M. Thomas, 2017: Characterizing the chaotic nature of ocean ventilation. *J. Geophys. Res. Oceans*, **122**, 7577–7594, https://doi.org/10.1002/2017JC012875.

——, H. L. Johnson, C. Lique, and D. P. Marshall, 2021: Demons in the North Atlantic: Variability of deep ocean ventilation. *Geophys. Res. Lett.*, **48**, e2020GL092340, https://doi.org/10.1029/2020GL092340.

MacKinnon, J. A., M. H. Alford, R. Pinkel, J. Klymak, and Z. Zhao, 2013: The latitudinal dependence of shear and mixing in the Pacific transiting the critical latitude for PSI. *J. Phys. Oceanogr.*, **43**, 3–16, https://doi.org/10.1175/JPO-D-11-0107.1.

Marshall, J. C., R. G. Williams, and A. G. Nurser, 1993: Inferring the subduction rate and period over the North Atlantic. *J. Phys. Oceanogr.*, **23**, 1315–1329, https://doi.org/10.1175/1520-0485(1993)023<1315:ITSRAP>2.0.CO;2.

Munk, W., and C. Wunsch, 1998: Abyssal recipes II: Energetics of tidal and wind mixing. *Deep-Sea Res. I*, **45**, 1977–2010, https://doi.org/10.1016/S0967-0637(98)00070-3.

Naveira Garabato, A. C., R. Ferrari, and K. L. Polzin, 2011: Eddy stirring in the Southern Ocean. *J. Geophys. Res.*, **116**, C09019, https://doi.org/10.1029/2010JC006818.

——, K. L. Polzin, R. Ferrari, J. D. Zika, and A. Forryan, 2016: A microscale view of mixing and overturning across the Antarctic Circumpolar Current. *J. Phys. Oceanogr.*, **46**, 233–254, https://doi.org/10.1175/JPO-D-15-0025.1.

Oakey, N. S., 1982: Determination of the rate of dissipation of turbulent energy from simultaneous temperature and velocity shear microstructure measurements. *J. Phys. Oceanogr.*, **12**, 256–271, https://doi.org/10.1175/1520-0485(1982)012<0256:DOTROD>2.0.CO;2.

Oltmanns, M., N. P. Holliday, J. Screen, B. I. Moat, S. A. Josey, D. G. Evans, and S. Bacon, 2024: European summer weather linked to North Atlantic freshwater anomalies in preceding years. *Wea. Climate Dyn.*, **5**, 109–132, https://doi.org/10.5194/wcd-5-109-2024.

Orúe-Echevarría, D., K. L. Polzin, A. C. Naveira Garabato, A. Forryan, and J. L. Pelegrí, 2023: Mixing and overturning across the Brazil-Malvinas Confluence. *J. Geophys. Res. Oceans*, **128**, e2022JC018730, https://doi.org/10.1029/2022JC018730.

Osborn, T. R., 1980: Estimates of the local rate of vertical diffusion from dissipation measurements. *J. Phys. Oceanogr.*, **10**, 83–89, https://doi.org/10.1175/1520-0485(1980)010<0083:EOTLRO>2.0.CO;2.

——, and C. S. Cox, 1972: Oceanic fine structure. *Geophys. Fluid Dyn.*, **3**, 321–345, https://doi.org/10.1080/03091927208236085.

Piccolroaz, S., B. Fernández-Castro, M. Toffolon, and H. A. Dijkstra, 2021: A multi-site, year-round turbulence microstructure atlas for the deep perialpine Lake Garda. *Sci. Data*, **8**, 188, https://doi.org/10.1038/s41597-021-00965-0.

Polzin, K. L., J. M. Toole, J. R. Ledwell, and R. W. Schmitt, 1997: Spatial variability of turbulent mixing in the abyssal ocean. *Science*, **276**, 93–96, https://doi.org/10.1126/science.276.5309.93.

——, A. C. Naveira Garabato, T. N. Huussen, B. M. Sloyan, and S. Waterman, 2014: Finescale parameterizations of turbulent dissipation. *J. Geophys. Res. Oceans*, **119**, 1383–1419, https://doi.org/10.1002/2013JC008979.

Prandtl, L., 1925: 7. Bericht über untersuchungen zur ausgebildeten turbulenz. *Z. Angew. Math. Mech.*, **5**, 136–139, https://doi.org/10.1002/zamm.19250050212.

Robbins, P. E., J. F. Price, W. B. Owens, and W. J. Jenkins, 2000: The importance of lateral diffusion for the ventilation of the lower thermocline in the subtropical North Atlantic. *J. Phys. Oceanogr.*, **30**, 67–89, https://doi.org/10.1175/1520-0485(2000)030<0067:TIOLDF>2.0.CO;2.

Roch, M., P. Brandt, S. Schmidtko, and F. P. Tuchen, 2024: Impact of the North Atlantic Oscillation on the decadal variability of the upper subtropical-tropical Atlantic Ocean. *J. Geophys. Res. Oceans*, **129**, e2023JC020614, https://doi.org/10.1029/2023JC020614.

Rudnickas, J., D. Palter Jr., D. Hebert, and H. T. Rossby, 2019: Isopycnal mixing in the North Atlantic Oxygen Minimum Zone revealed by RAFOS floats. *J. Geophys. Res Oceans*, **124**, 6478–6497, https://doi.org/10.1029/2019JC015148.

Schmit, R. W., J. M. Toole, R. L. Koehler, E. C. Mellinger, and K. W. Doherty, 1988: The development of a fine- and microstructure profiler. *J. Atmos. Oceanic Technol.*, **5**, 484–500, https://doi.org/10.1175/1520-0426(1988)005<0484:TDOAFA>2.0.CO;2.

Sheen, K. L., and Coauthors, 2014: Eddy-induced variability in Southern Ocean abyssal mixing on climatic timescales. *Nat. Geosci.*, **7**, 577–582, https://doi.org/10.1038/ngeo2200.

Sijp, W. P., M. Bates, and M. H. England, 2006: Can isopycnal mixing control the stability of the thermohaline circulation in ocean climate models? *J. Climate*, **19**, 5637–5651, https://doi.org/10.1175/JCLI3890.1.

Spingys, C. P., R. G. Williams, R. E. Tuerena, A. Naveira Garabato, C. Vic, A. Forryan, and J. Sharples, 2021: Observations of nutrient supply by mesoscale eddy stirring and small-scale turbulence in the oligotrophic North Atlantic. *Global Biogeochem. Cycles*, **35**, e2021GB007200, https://doi.org/10.1029/2021GB007200.

Stommel, H., 1979: Determination of water mass properties of water pumped down from the Ekman layer to the geostrophic flow below. *Proc. Natl. Acad. Sci. USA*, **76**, 3051–3055, https://doi.org/10.1073/pnas.76.7.3051.

Tulloch, R., and Coauthors, 2014: Direct estimate of lateral eddy diffusivity upstream of Drake Passage. *J. Phys. Oceanogr.*, **44**, 2593–2616, https://doi.org/10.1175/JPO-D-13-0120.1.

Voet, G., H. Drake, and J. Cusack, 2023: modscripps/mixsea V0.1.2. Zenodo, accessed 8 February 2024, https://doi.org/10.5281/zenodo.10636077.

Waterhouse, A. F., and Coauthors, 2014: Global patterns of diapycnal mixing from measurements of the turbulent dissipation rate. *J. Phys. Oceanogr.*, **44**, 1854–1872, https://doi.org/10.1175/JPO-D-13-0104.1.

Weller, R. A., P. W. Furey, M. A. Spall, and R. E. Davis, 2004: The large-scale context for oceanic subduction in the Northeast Atlantic. *Deep-Sea Res. I*, **51**, 665–699, https://doi.org/10.1016/j.dsr.2004.01.003.

Whalen, C. B., L. D. Talley, and J. A. MacKinnon, 2012: Spatial and temporal variability of global ocean mixing inferred from Argo profiles. *Geophys. Res. Lett.*, **39**, L18612, https://doi.org/10.1029/2012GL053196.

——, J. A. MacKinnon, and L. D. Talley, 2018: Large-scale impacts of the mesoscale environment on mixing from wind-driven internal waves. *Nat. Geosci.*, **11**, 842–847, https://doi.org/10.1038/s41561-018-0213-6.

Williams, R. G., 1991: The role of the mixed layer in setting the potential vorticity of the main thermocline. *J. Phys. Oceanogr.*, **21**, 1803–1814, https://doi.org/10.1175/1520-0485(1991)021<1803:TROTML>2.0.CO;2.

——, J. C. Marshall, and M. A. Spall, 1995: Does Stommel's mixed layer "demon" work? *J. Phys. Oceanogr.*, **25**, 3089–3102, https://doi.org/10.1175/1520-0485(1995)025<3089:DSMLW>2.0.CO;2.

Wong, A. P., and Coauthors, 2020: Argo data 1999–2019: Two million temperature-salinity profiles and subsurface velocity observations from a global array of profiling floats. *Front. Mar. Sci.*, **7**, 700, https://doi.org/10.3389/fmars.2020.00700.

Zika, J. D., T. J. McDougall, and B. M. Sloyan, 2010: Weak mixing in the eastern North Atlantic: An application of the tracer-contour inverse method. *J. Phys. Oceanogr.*, **40**, 1881–1893, https://doi.org/10.1175/2010JPO4360.1.